# Mechanism of aniline adsorption on post-crosslinked resins: pore structure and oxygen content

Wenhao Yu, Chao Xu, Chai Yin, Shitao Yu, Weizhi Sun, Congxia Xie and Mo Xian

## ABSTRACT

A series of post-crosslinked resins were synthesized from macroporous chloromethylated styrene-divinylbenzene copolymer by controlling post-crosslinked reaction conditions. Adsorption study towards aniline showed that the three resins, ST-DVB-WH5, ST-DVB-WH6, and ST-DVB-WH7, prepared at different temperatures, and which had nearly identical static adsorption capacity, displayed great disparity in kinetic behavior. The rate constant of ST-DVB-WH7 by the pseudo-first-order model was 1.50 and 1.19 times higher than that of ST-DVB-WH5 and ST-DVB-ST-DVB-WH6. Further analysis of the diffusion model showed that the three resins exhibited different diffusion rates due to the difference in oxygen content and pore structure of each resin. The results showed that the adsorption capacity was mainly decided by the pore volume within 1.14 and 3.42 nm and the adsorption rate was mainly decided by the oxygen content of the resin. In addition, as the best synthetic resin for aniline adsorption, the equilibrium adsorption capacity of ST-DVB-WH7 was 1.57 times and 1.44 times higher than that of H-103 and NKA-II, respectively.

**Key words** | adsorption, aniline, diffusion model, post-crosslinked resin

**Wenhao Yu**
**Chai Yin**
**Shitao Yu**
**Congxia Xie** (corresponding author)
School of Chemical Engineering,
Qingdao Science and Technology University,
Qingdao 266042,
China
E-mail: *xiecongxia@126.com*

**Wenhao Yu**
**Chao Xu**
**Chai Yin**
**Weizhi Sun**
**Mo Xian**
Key Laboratory of Biobased Materials,
Qingdao Institute of Bioenergy and Bioprocess Technology, Chinese Academy of Sciences,
Qingdao 266101,
China

## INTRODUCTION

Aniline, as a typical organic intermediate, is widely applied in pharmacy, dyes, rubber production and so on (An *et al.* 2009). However, the use of aniline is accompanied by the discharge of aniline-containing wastewater. This not only causes environmental pollution, but also wastes resources. Hence, it is of great significance to explore an effective strategy for the recovery of aniline from sewage and it has also attracted vast attention in recent years (An *et al.* 2009).

Many methods have been proposed for the treatment of wastewater, such as a biological process (Cui *et al.* 2017), photo-catalysis (Sánchez *et al.* 1998), extraction (Ebrahimpour *et al.* 2017), electrolysis (Li *et al.* 2017), adsorption (Chen *et al.* 2017) and some other processes. For the present, adsorption is an efficient processing technology for treating wastewater, which has the advantages of simple operation, flexibility and high adsorption capacity (Iannicelli-Zubiani *et al.* 2018; Norouzi *et al.* 2018). As the most frequently used adsorbent, adsorption resin has the advantages of high specific surface area, high adsorption capacity and good design ability (Zhang & Huang 2017). It has become the focus of some researchers because of its good application prospects in wastewater treatment.

Aniline is an aromatic compound with medium polarity, and the proper polarity is advantageous for the adsorption toward aniline onto the adsorbent. The macroporous chloromethylated styrene-divinylbenzene copolymer (CMPS) is often used as a precursor resin for the post-crosslinked resin synthesis, and this kind of post-crosslinked resin, which was synthesized from CMPS, exhibits a high specific surface area and excellent sorption properties (Ahn *et al.* 2006; Li *et al.* 2016). During the synthesis process of post-crosslinked resin, different contents of oxygen-containing groups are formed through oxidation by nitrobenzene with different reaction conditions. This would definitely enhance the polarity of the material as well as providing some chemical interacting sites for aniline, which is advantageous for the adsorption of aniline. Therefore, the oxygen-containing post-crosslinked resin has huge advantages in the adsorption of aniline because of its good physical structure and its appropriate polarity. The synthesis of oxygen-containing post-crosslinked resins

doi: 10.2166/wst.2018.484

has been reported (Li *et al.* 2016), but no detailed mechanism study was carried out.

Hence, in this paper, a series of post-crosslinked resins with different structures was synthesized from the CMPS by controlling the Friedel-Crafts reaction condition. Subsequently, several resins (ST-DVB-WH5, ST-DVB-WH6 and ST-DVB-WH7) with good adsorption performances were screened by contrastive analysis of the static adsorption result. An exhaustively detailed study of the adsorption mechanism was performed by diffusion model analysis. Eventually, in order to reflect the significance of the experiment, comparison of the adsorption capacity of aniline between the best synthetic resin and the commercial resin was carried out.

## EXPERIMENTS

### Chemicals and materials

CMPS was obtained from Tianjin Yunneng Co., Ltd. H-103 was supplied by Zhengzhou Qinshi Co., Ltd. Anhydrous aluminum chloride ($AlCl_3$), anhydrous ferric chloride ($FeCl_3$), anhydrous zinc chloride ($ZnCl_2$), nitrobenzene ($C_6H_5NO_2$) and aniline were obtained from Sinopharm Chemical Reagent Co., Ltd. All reagents used in the present investigation were analytical reagents and used without further purification.

### Preparation of the post-crosslinked resins

Typically, in a three-necked round-bottomed flask, 20.0 g of CMPS was swollen with mechanical agitation overnight in 100 mL of nitrobenzene. 4.0 g of catalyst was added to the system at a given temperature. The reaction mixture was reacted for 12 h. When the reaction was completed, the mixture was cooled to room temperature and the resin was washed with ethanol and water, respectively, to remove residual solvent and catalyst. Finally, these resins were dried in the air dry oven at 333 K for 12 h and WH series resins were obtained. The synthetic equation is illustrated in Figure 1.

### Experiment on static adsorption capacity

A 250 mL conical flask with stopper was loaded with 0.1 g of resins and 100 mL of aniline at the initial concentration of 500 mg/L. Then, it was placed in a thermostatic oscillator for 12 h to ensure that the adsorption equilibrium was reached. According to the formula, the adsorption capacity $Q_e$ of aniline by the resins (mg/g) was calculated. The formula was:

$$Q_e = (C_0 - C_e)V/M \tag{1}$$

Here $Q_e$ is the equilibrium capacity (mg/g), $C_0$ and $C_e$ are the initial and equilibrium concentration (mg/L). $V$ is the volume of the solution (L), and $M$ is the quality of the resin (g).

### Adsorption kinetic

For kinetic adsorption, about 0.1 g of resins were added into 100 mL of aniline aqueous system (1,000 mg/L) in a conical flask, and then this was placed in a thermostatic oscillator at 303 K for adsorption until equilibrium was reached. During the adsorption process, systems were sampled at preset time intervals and the residual concentration of the adsorbate was monitored. According to the formula, the adsorption capacity $Q_t$ of aniline by the resins (mg/g) was calculated. The formula was:

$$Q_t = (C_0 - C_t)V/M \tag{2}$$

Here, $Q_t$ is the capacity at contact time (mg/g), and $C_t$ is the concentration of PABA at contact time (mg/L).

### Adsorption isotherms

A 250 mL conical flask with stopper was loaded with 0.1 g of resins and 100 mL of aniline at the initial concentration

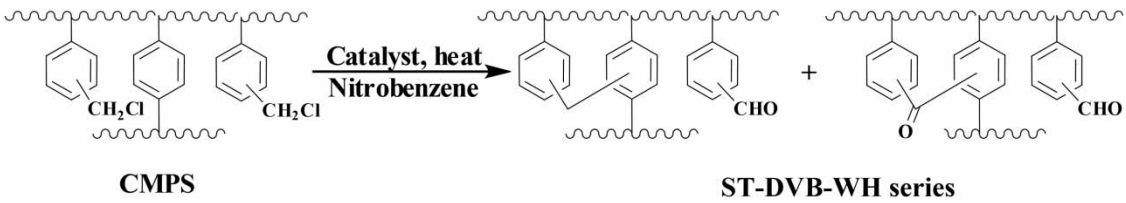


**Figure 1** | Schematic procedure for synthesis of ST-DVB-WH series resins.

of 100 mg/L, 200 mg/L, 500 mg/L, 800 mg/L and 1,000 mg/L, respectively. Then placed it in a thermostatic oscillator at 303 K with 12 h to ensure that the adsorption equilibrium was reached. The adsorption capacity $Q_e$ of aniline by the resins (mg/g) was calculated as formula (1).

### Analysis

The residual chlorine content of the resins was measured by the Volhard method. The synthesized resins were characterized by Fourier transform infrared spectroscopy (FT-IR Nicolet iN10 IR Microscope, Thermo Fisher, USA) and $N_2$ adsorption analysis (ASAP2020 M + C, Micromeritics, USA). The concentration of aniline in the aqueous solution was determined by UV-Vis spectrophotometer (Varian). The scanning electron microscopy (SEM) and energy dispersive X-ray (EDX) analysis of the resins was obtained with a high-performance scanning electron microscope (Hitachi, S-4800, Japan). The elemental analysis of the resins was obtained with a Vario EL III Elementar Analysensysteme (Elementar, Germany) and the oxygen content was calculated by the following formula: 100% = C% + O% + Cl% + H% (Kuang *et al.* 2017).

## RESULTS AND DISCUSSION

### Characterization and static adsorption capacity of resins

The IR spectra of ST-DVB-WH series and CMPS are shown in Figure 2. As the synthetic temperature increased, the band at 1,265 $cm^{-1}$ which was assigned to the -$CH_2Cl$ bond (bending vibration of C-Cl) sharply decreased (Wang *et al.* 2017b). A new peak at 1,710 $cm^{-1}$ appeared at different temperatures, and it represented the -C = O band of the formaldehyde carbonyl group (Yu *et al.* 2018). Besides, it is worthwhile mentioning that an obvious band at 1,650 $cm^{-1}$ that was assigned to the -C = O vibration of the ketone carbonyl groups emerged on resins ST-DVB-WH4 and ST-DVB-WH7 (Wang *et al.* 2016). These carbonyl vibration bands might come from the oxidation of -$CH_2Cl$ groups on CMPS and catalyst $FeCl_3$ or high-temperature could bring about serious oxidation.

The preparation conditions of these resins and the results of the static adsorption behavior of these resins toward aniline are shown in Table 1. Catalysts played a significant role in the adsorption performances. Although the ST-DVB-WH1 and ST-DVB-WH4 resins were prepared at 353 K, they displayed lower static adsorption capacity than

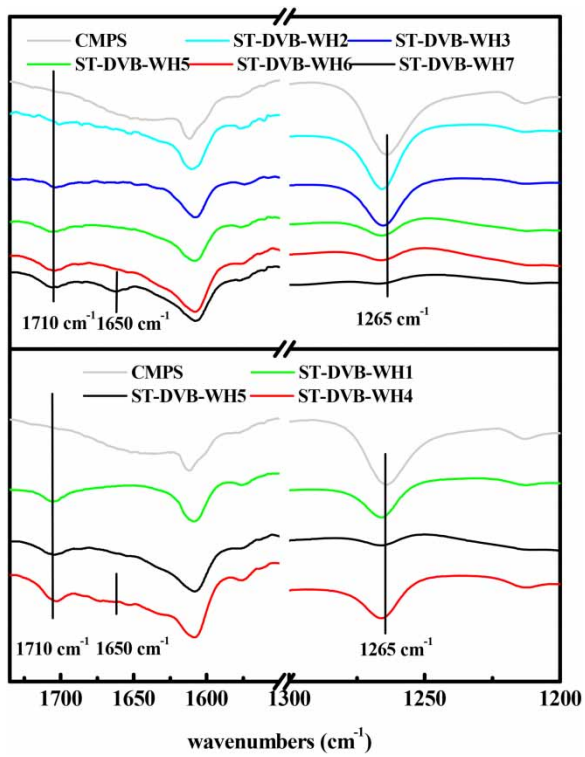


**Figure 2** | IR spectra of ST-DVB-WH series resins.

**Table 1** | Reaction condition with ST-DVB-WH series resins

| Resin | Tempreature | Catalyst | $Q_e$ (mg/g) |
|---|---|---|---|
| ST-DVB-WH1 | 80 | $ZnCl_2$ | 116.3 |
| ST-DVB-WH2 | 40 | $AlCl_3$ | 182.6 |
| ST-DVB-WH3 | 60 | $AlCl_3$ | 198.1 |
| ST-DVB-WH4 | 80 | $FeCl_3$ | 207.1 |
| ST-DVB-WH5 | 80 | $AlCl_3$ | 243.4 |
| ST-DVB-WH6 | 100 | $AlCl_3$ | 238.9 |
| ST-DVB-WH7 | 120 | $AlCl_3$ | 242.2 |

that of ST-DVB-WH5. This could be attributed to their poor specific surface area. In our earlier studies, the specific surface area of these resins, which were prepared through $ZnCl_2$ and $FeCl_3$ as catalysts, exhibited a low value (Wang *et al.* 2017a).

The influence of temperature is a little complicated. When the reaction temperature was below 353 K, the adsorption capacity increased as the synthetic temperature increased and it reached the highest point at 353 K. The adsorption capacity did not change with further increases in reaction temperature. This is not consistent with a previous report, in which obvious increment in adsorption

was observed with elevated temperature (Han *et al.* 2017). Hence, ST-DVB-WH5, ST-DVB-WH6 and ST-DVB-WH7 were considered as the key to research, and detailed studies on the physical structure and oxygen content of the three resins were carried out.

The adsorption and desorption isotherms of $N_2$ on the screened resins are shown in Figure 3(a). At the initial part of the isotherm (the relative pressure below 0.1), the adsorption capacity increased sharply with the increment of relative pressure, then it displayed a gentle trend and it could be deemed that there were a large number of micropores and a small number of mesopores in the resins. Subsequently, in the final part of the isotherm (relative pressure below 0.9), the adsorption capacity increased sharply with the increment of relative pressure, and it indicated that there still existed a number of macropores in the resins. In terms of details, the higher the reaction temperature was, the more thorough the Friedel-Crafts reaction was. In other words, the number of mesopores and macropores decreased as the reaction temperature increased and this trend was perfectly reflected in Figure 3(b).

In previous studies, the optimal ratio of the pore diameter of the resin to the molecular size of the adsorbate was 2–6 times and it played an extremely important part in adsorption (Huang *et al.* 2008). It is worth mentioning that the size of aniline was calculated as 0.57 nm*0.43 nm (the optimal molecular size of aniline was calculated based on the bond length and the bond angle by the ChemBioOffice 2010 software, and the information on the bond length and the bond angle is displayed in Figure S1, available with the online version of this paper). As is shown in Table 2, three resins, ST-DVB-WH5, ST-DVB-WH6 and ST-DVB-WH7, which reacted at different temperatures, had a nearly equal volume of effective adsorption pores with 1.14 nm and 3.42 nm, while the oxygen contents were quite different. Hence, these generated oxygen-containing functional

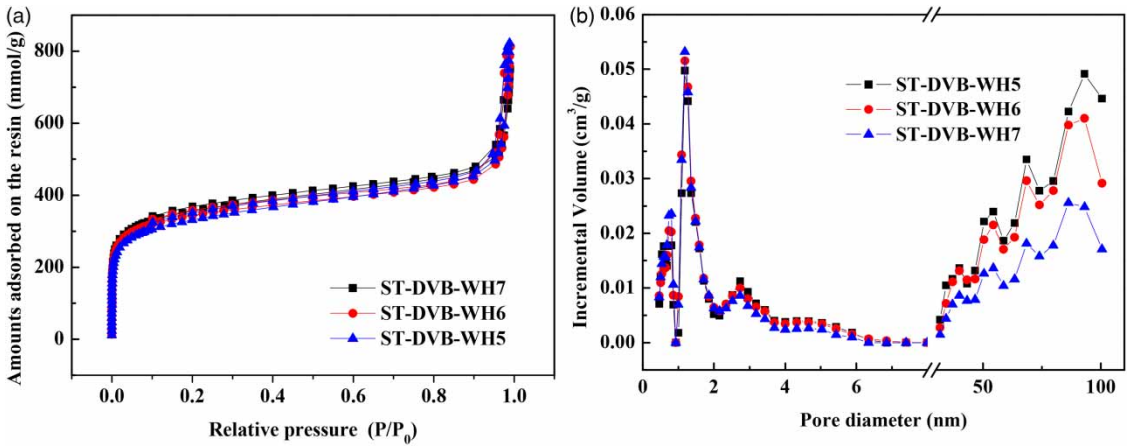


**Figure 3** | $N_2$ adsorption-desorption isotherms (a) and pore size distribution vs incremental volume (b) of ST-DVB-WH5, ST-DVB-WH6 and ST-DVB-WH7.

**Table 2** | The analysis of the structure of ST-DVB-WH5, ST-DVB-WH6 and ST-DVB-WH7

| | Adsorbent | | | | |
|---|---|---|---|---|---|
| | **ST-DVB-WH5** | **ST-DVB-WH6** | **ST-DVB-WH7** | **H-103** | **NKA-II** |
| BET surface area ($m^2$/g) | 1,226.9 | 1,280.1 | 1,322.9 | 1,187.3 | 1,060.7 |
| Micropore surface area ($m^2$/g) | 729.8 | 753.2 | 792.8 | 779.6 | 606.9 |
| Micropore volume ($cm^3$/g) | 0.34 | 0.36 | 0.37 | 0.34 | 0.28 |
| Pore volume ($cm^3$/g) 1.14 nm < D < 3.42 nm | 0.1833 | 0.1837 | 0.1865 | 0.1531 | 0.1393 |
| 2 nm < D < 6 nm | 0.0780 | 0.0756 | 0.0739 | 0.0459 | 0.0558 |
| Chlorine content (%) | 3.11 | 2.49 | 1.42 | – | – |
| Oxygen content (%) | 3.55 | 5.31 | 7.51 | – | – |

groups appeared to have little or no effect on the adsorption capacity. For further study on the influence of oxygen, adsorption kinetic experiments were performed.

## Mechanism of aniline adsorption on ST-DVB-WH5, ST-DVB-WH6 and ST-DVB-WH7

Figure 4 displays the kinetic curves of adsorption of aniline from aqueous solution onto ST-DVB-WH5, ST-DVB-WH6 and ST-DVB-WH7. Obviously, the adsorption of aniline onto these resins could reach adsorption equilibrium within 300 min. The pseudo-first-order and pseudo-second-order kinetic models were used to investigate the adsorption kinetics of aniline, and it could be determined as (Javadian *et al.* 2014; Naushad *et al.* 2017):

$$\ln(Q_e - Q_t) = \ln Q_e - K_1 t \tag{3}$$

$$t/Q_t = 1/K_2 Q_e^2 + t/Q_e \tag{4}$$

Here, $K_1$ ($min^{-1}$) and $K_2$ (g/(mg·min)) are the pseudo-first-order and pseudo-second-order rate constants, respectively.

According to the results of curve fitting (Table 3 and Figure 4), the pseudo-first-order model was more suitable for all resins because of its higher fitting correlation parameters ($R^2 > 0.98$). The rate constant $K_1$ followed the sequence: ST-DVB-WH7 > ST-DVB-WH6 > ST-DVB-WH5, indicating that the rate of adsorption toward aniline also followed the sequence: ST-DVB-WH7 > ST-DVB-WH6 > ST-DVB-WH5. However, although these three resins had different adsorption rates and physical properties, the maximal equilibrium adsorption capacity at this initial concentration did not have an obvious gap. Hence, it was

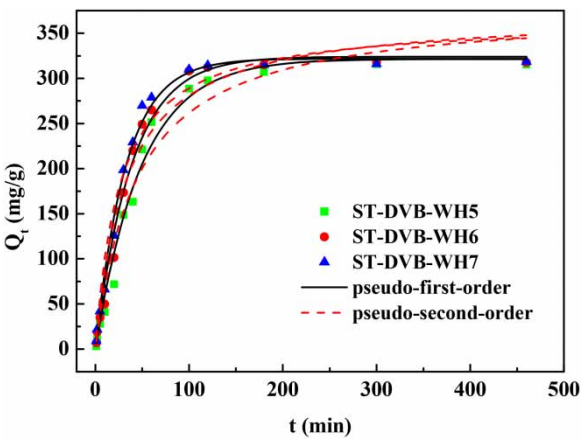


**Figure 4** | The adsorption kinetics of ST-DVB-WH5, ST-DVB-WH6 and ST-DVB-WH7.

**Table 3** | The fitting of the adsorption kinetics models of WH resins

| | Pseudo-first-order model | | Pseudo-second-order model | |
|---|---|---|---|---|
| **Adsorbents** | $K_1(10^{-3})$ | $R^2$ | $K_2(10^{-5})$ | $R^2$ |
| ST-DVB-WH5 | 20.29 | 0.9840 | 5.98 | 0.9611 |
| ST-DVB-WH6 | 25.76 | 0.9889 | 8.24 | 0.9626 |
| ST-DVB-WH7 | 30.57 | 0.9926 | 10.47 | 0.9668 |

necessary to study the film model and intra-particle model. The film diffusion model and intra-particle diffusion model could be determined as (Islam *et al.* 2015):

$$\ln(1 - F) = -k_f t \tag{5}$$

$$k_p = Q_t/t^{1/2} \tag{6}$$

Here, $k_f$ ($min^{-1}$) and $F = (Q_t/Q_e)$ are the film diffusion rate parameter and the fractional attainment of equilibrium and $k_p$ is the intra-particle diffusion rate parameter ([(mg/g)/$(min)^{1/2}$]).

As is shown in Figure 5(a) and Table S1 (available with the online version of this paper), the film diffusion rate of the resin followed the sequence ST-DVB-WH7 > ST-DVB-WH6 > ST-DVB-WH5. According to the results of elemental analysis, it was found that the oxygen content of these resins also conformed to this sequence because these hydrophilic groups, which are formed by the O element, increased the affinity to the bulk aqueous phase. This may facilitate the interaction between the surface of the resin and the adsorbate molecule, contributing a larger film diffusion rate in the film diffusion stage (Yu *et al.* 2004).

At the intra-particle diffusion stage, it can be observed in Figure 5(b) that the three resins exhibited a platform tendency in the initial stage. The ST-DVB-WH7 resin converged towards a linear function and ST-DVB-WH5 converged towards a quadratic function, indicating that the diffusion rate of the ST-DVB-WH5 resin increased slowly, while that of the ST-DVB-WH7 resin increased rapidly. Subsequently, ST-DVB-WH5 acquired a higher diffusion rate until 20 minutes later and the intra-particle diffusion rate of the resin followed the sequence ST-DVB-WH5 > ST-DVB-WH6 > ST-DVB-WH7 (Table S1). This was similar to the ordering of the mesopores within the size range of 2–6 nm (Wang *et al.* 2017a). This might be because after the resin was completely wetted, it had a high mass transfer driving force which was induced to the high concentration of the solution in the initial stage. Hence, the pore volume of 2–6 nm played a crucial role in the intra-particle diffusion. In the

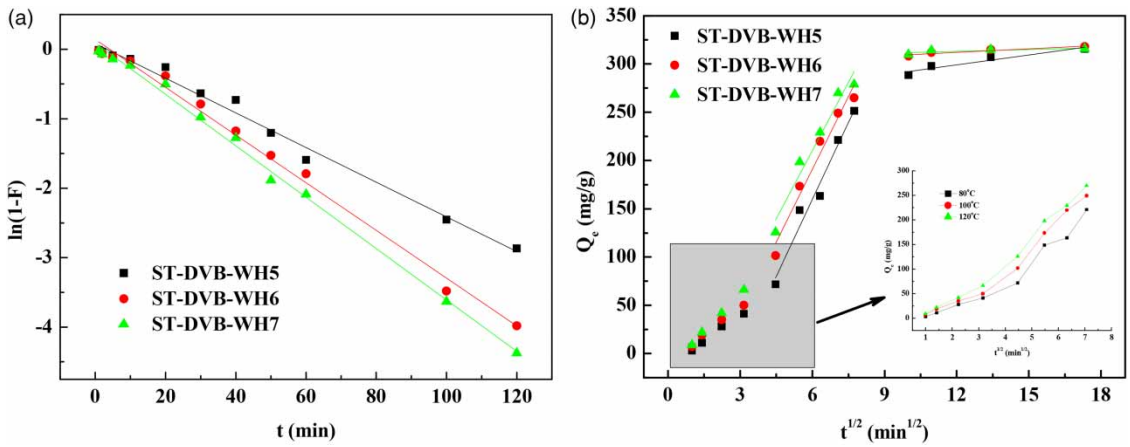


**Figure 5** | The fitting of the film diffusion model (a) and intra-particle diffusion model (b) of ST-DVB-WH5, ST-DVB-WH6 and ST-DVB-WH7.

final stage, the fitting line tended to level, indicating that the adsorption equilibrium was reached. Besides, if $Q_t$ shows a multi-linear relationship with the $t^{1/2}$ curve or the fitting line does not pass through the origin, then two or more stages will affect the adsorption (Yu *et al.* 2018). Obviously, all the resins gave straight lines that did not pass through the origin, indicating that both the film diffusion and the intra-particle diffusion were the rate-limiting steps. The best synthetic resin, ST-DVB-WH7, for aniline adsorption was used to compare with the commercial resins.

## Comparison of adsorption performance with ST-DVB-WH7 and commercial resins

In order to compare the adsorption capacity of ST-DVB-WH7 with the commercial resins H-103 and NKA-II toward aniline, the adsorption kinetics and isotherm were studied. As is shown in Table S2 and Figure 6, although ST-DVB-WH7 did not have advantages in adsorption rate, the intra-particle diffusion rate of ST-DVB-WH7 was 2.04 times and 2.37 times higher than that of NKA-II and H-103, respectively. Adsorption isotherms of aniline adsorption onto ST-DVB-WH7, NKA-II and H-103 in aqueous solution at 303 K are shown in Figure 7; the Langmuir model fitted the isotherm better because of its larger correlation coefficient (Table S3), and equilibrium adsorption capacity toward aniline was 1.57 times and 1.44 times higher than that of commercial resins H-103 and NKA-II. (Tables S2 and S3 are available with the online version of this paper.)

According to a comparative study of the physical properties of the resins (Table 2), it was found that on the point of the micropore surface area, there was not an obvious gap between H-103 and ST-DVB-WH7, but on the point of

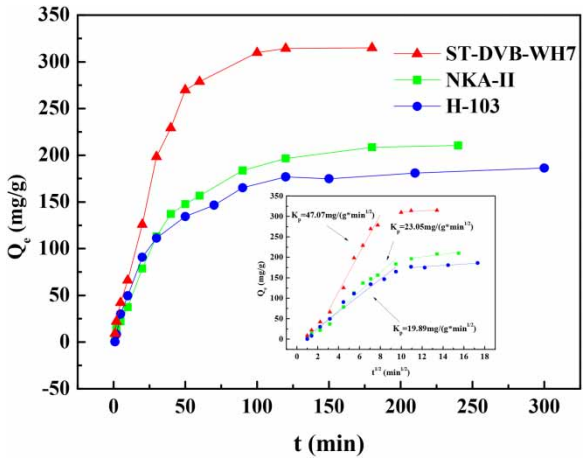


**Figure 6** | The result of the adsorption kinetics and intra-particle diffusion model of ST-DVB-WH7, NKA-II and H-103.

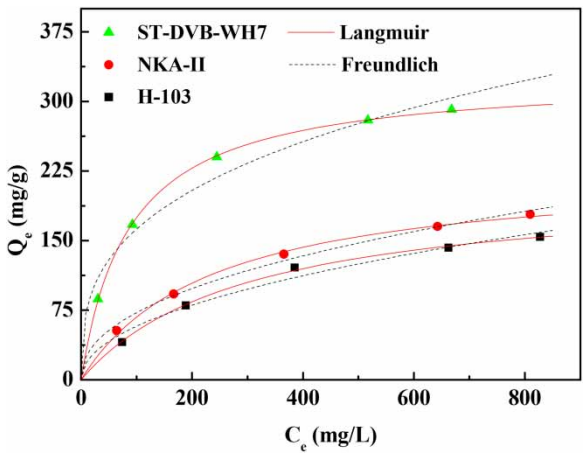


**Figure 7** | The result of the adsorption isotherm of ST-DVB-WH7, NKA-II and H-103.

effective pore volume (1.14 nm–3.42 nm), ST-DVB-WH7 displayed a greater advantage than H-103. On the other hand, although NKA-II had a polar surface structure, its physical properties including micropore surface area, Brunauer–Emmett–Teller (BET) surface area and effective pore volume were much lower than those of ST-DVB-WH7. However, the dipole moment of aniline was $1.51*10^{-30}$ (C*m) (Qin *et al.* 2006), demonstrating that aniline is a medium polarity organic compound and adsorption toward aniline onto adsorbents depends mainly on physical interaction. In general, the polar surface structure played a crucial role in aniline adsorption at the same level as physical properties. Otherwise, the physical properties, especially in terms of effective pore volume, became the most significant factor in aniline adsorption. Similarly, ST-DVB-WH7 also displayed a higher intra-particle diffusion rate due to its higher pore volume (2 nm < D < 6 nm).

### Changes before and after adsorption

Figure S2 shows the FT-IR results of ST-DVB-WH7 before adsorption of aniline and after adsorption of aniline. The two main vibrational bands of ST-DVB-WH7 could be assigned as 1,710 $cm^{-1}$ (formaldehyde carbonyl groups) and 1,650 $cm^{-1}$ (ketone carbonyl groups). After adsorption of aniline, the vibrational bands of formaldehyde and ketone carbonyl groups appeared red-shifted. In general, the presence of red-shift demonstrated the presence of the interaction between the group and the adsorbate. On the other hand, there were two typical vibrational bands which appeared at 1,619 $cm^{-1}$ and 749 $cm^{-1}$, indicating the successful adsorption of aniline onto the resin. Moreover, Figure S3 shows the SEM results of aniline adsorption onto ST-DVB-WH7 (before and after adsorption). It can be seen in Figure S3(a) that the surface of the resin was rough and more pores can be seen, indicating that the pore volume of the resin was large. Figure S2(b) shows that the surface of the resin was smooth, indicating that the pore volume of the resin was small. This might be due to the micropore filling effect, which caused the pores to be filled with aniline molecules. (Figures S2 and S3 are available with the online version of this paper.)

## CONCLUSION

A series of post-crosslinked resins were synthesized by carefully controlled post crosslinking reactions from CMPS. Three resins, ST-DVB-WH5, ST-DVB-WH6 and ST-DVB-WH7, prepared under $AlCl_3$ at different temperatures, were screened for the adsorption of aniline and these resins displayed similar static adsorption capacity due to their nearly identical pore volume within pore diameters between 1.14 and 3.42 nm. The adsorption kinetics showed that the pseudo-first-order model was more suitable for the three resins, and ST-DVB-WH7 displayed the highest rate constant. Further investigation of diffusion models showed that ST-DVB-WH7 displayed the highest film diffusion rate and ST-DVB-WH5 displayed the highest intra-particle diffusion rate. Although the oxygen content of the resin posed no impact on the adsorption capacity of aniline, it posed a huge influence on the film diffusion rate. In addition, the pore volume within pore diameters between 1.14 nm and 3.42 nm played a key role in the adsorption capacity of aniline. ST-DVB-WH7 exhibited the best adsorption performance in the synthetic resins and the equilibrium adsorption capacity toward aniline was 1.57 times and 1.44 times higher than that of commercial resins H-103 and NKA-II.

## ACKNOWLEDGEMENTS

The research was supported by the Taishan Scholars Construction Projects of Shandong (ts201511033) and Natural Science Foundation of Shandong Province (ZR2016BQ39). Authors Wenhao Yu and Chao Xu contributed equally to this work.

## REFERENCES

Ahn, J., Jang, J., Oh, C., Ihm, S., Cortez, J. & Sherrington, D. C. 2006 Rapid generation and control of microporosity, bimodal pore size distribution, and surface area in Davankov-type hyper-cross-linked resins. *Macromolecules* **39** (2), 627–632.

An, F., Feng, X. & Gao, B. 2009 Adsorption of aniline from aqueous solution using novel adsorbent PAM/SiO2. *Chemical Engineering Journal* **151** (1–3), 183–187.

Chen, C., Geng, X. & Huang, W. 2017 Adsorption of 4-chlorophenol and aniline by nanosized activated carbons. *Chemical Engineering Journal* **327**, 941–952.

Cui, D., Shen, D., Wu, C., Li, C., Leng, D. & Zhao, M. 2017 Biodegradation of aniline by a novel bacterial mixed culture AC. *International Biodeterioration & Biodegradation* **125**, 86–96.

Ebrahimpour, E., Amiri, A., Baghayeri, M., Rouhi, M. & Lakouraj, M. M. 2017 Poly(indole-co-thiophene)@Fe3O4 as novel adsorbents for the extraction of aniline derivatives from water samples. *Microchemical Journal* **131**, 174–181.

Han, F., Xu, C., Sun, W., Yu, S. & Xian, M. 2017 Effective removal of phenolic compounds by a newly-synthesized adsorption

resin: behavior and mechanism. *Ion Exchange & Adsorption* **33** (1), 32–45.

Huang, J.-H., Huang, K.-L., Liu, S.-Q., Wang, A. T. & Yan, C. 2008 Adsorption of rhodamine B and methyl orange on a hypercrosslinked polymeric adsorbent in aqueous solution. *Colloids and Surfaces A: Physicochemical and Engineering Aspects* **330** (1), 55–61.

Iannicelli-Zubiani, E. M., Gallo Stampino, P., Cristiani, C. & Dotelli, G. 2018 Enhanced lanthanum adsorption by amine modified activated carbon. *Chemical Engineering Journal* **341**, 75–82.

Islam, M., Mu, N. & Patel, R. 2015 Polyaniline/basic oxygen furnace slag nanocomposite as a viable adsorbent for the sorption of fluoride from aqueous medium: equilibrium, thermodynamic and kinetic study. *Desalination & Water Treatment* **54** (2), 450–463.

Javadian, H., Angaji, M. T. & Naushad, M. 2014 Synthesis and characterization of polyaniline/$\gamma$-alumina nanocomposite: a comparative study for the adsorption of three different anionic dyes. *Journal of Industrial & Engineering Chemistry* **20** (5), 3890–3900.

Kuang, W., Liu, Y. N. & Huang, J. 2017 Phenol-modified hyper-cross-linked resins with almost all micro/mesopores and their adsorption to aniline. *J. Colloid Interface Sci.* **487**, 31–37.

Li, X., Liu, Y., Di, D., Wang, G. & Liu, Y. 2016 A formaldehyde carbonyl groups-modified self-crosslinked polystyrene resin: synthesis, adsorption and separation properties. *Colloids and Surfaces A: Physicochemical and Engineering Aspects* **500**, 1–9.

Li, X., Jin, X., Zhao, N., Angelidaki, I. & Zhang, Y. 2017 Efficient treatment of aniline containing wastewater in bipolar membrane microbial electrolysis cell-Fenton system. *Water Research* **119**, 67–72.

Naushad, M., Ahamad, T., Al-Maswari, B. M., Alqadami, A. A. & Alshehri, S. M. 2017 Nickel ferrite bearing nitrogen-doped mesoporous carbon as efficient adsorbent for the removal of highly toxic metal ion from aqueous medium. *Chemical Engineering Journal* **330**, 1351–1360.

Norouzi, S., Heidari, M., Alipour, V., Rahmanian, O., Fazlzadeh, M., Mohammadi-Moghadam, F., Nourmoradi, H., Goudarzi, B. & Dindarloo, K. 2018 Preparation, characterization and Cr(VI) adsorption evaluation of NaOH-activated carbon produced from Date Press Cake; an agro-industrial waste. *Bioresource Technology* **258**, 48–56.

Qin, C., Hongying, L. I. & Guo, H. 2006 A new method of synthesize benzoic acid in experiment in fine organic synthesis. *Journal of Zhaoqing University* **27** (2), 47–49.

Sánchez, L., Peral, J. & Domènech, X. 1998 Aniline degradation by combined photocatalysis and ozonation. *Applied Catalysis B Environmental* **19** (1), 59–65.

Wang, X., Zhao, C., Zha, H., Huang, J. & Liu, Y. N. 2016 Post-crosslinked poly(meta-divinylbenzene) and its adsorption to phenol from aqueous solutions. *Journal of Nanoscience & Nanotechnology* **16** (7), 6810–6815.

Wang, C., Xu, C., Sun, W., Liu, F., Yu, S., Xian, M., Wang, C., Xu, C., Sun, W. & Liu, F. 2017a Effective adsorption of nitroaromatics at the low concentration by a newly-synthesized hypercrosslinked resin. *Water Science & Technology* **76** (9), 2328–2336.

Wang, X., Li, H. & Huang, J. 2017b Adsorption of *p*-chlorophenol on three amino-modified hyper-cross-linked resins. *J. Colloid Interface Sci.* **505**, 585–592.

Yu, Y., Zhuang, Y.-Y., Wang, Z.-H. & Qiu, M.-Q. 2004 Adsorption of water-soluble dyes onto modified resin. *Chemosphere* **54** (3), 425–430.

Yu, W., Sun, W., Xu, C., Wang, C., Jia, Y., Qin, X., Xie, C., Yu, S. & Xian, M. 2018 Effective adsorption toward p-aminobenzoic acid from aqueous solution by a L-malic acid modified hyper-crosslinked resin: equilibria and kinetics. *Journal of the Taiwan Institute of Chemical Engineers* **89**, 105–112.

Zhang, T. & Huang, J. 2017 N-vinylimidazole modified hyper-cross-linked resins and their adsorption toward Rhodamine B: effect of the cross-linking degree. *Journal of the Taiwan Institute of Chemical Engineers* **80**, 293–300.

First received 21 July 2018; accepted in revised form 12 November 2018. Available online 23 November 2018